

# RSC Advances



This is an *Accepted Manuscript*, which has been through the Royal Society of Chemistry peer review process and has been accepted for publication.

*Accepted Manuscripts* are published online shortly after acceptance, before technical editing, formatting and proof reading. Using this free service, authors can make their results available to the community, in citable form, before we publish the edited article. This *Accepted Manuscript* will be replaced by the edited, formatted and paginated article as soon as this is available.

You can find more information about *Accepted Manuscripts* in the [Information for Authors](#).

Please note that technical editing may introduce minor changes to the text and/or graphics, which may alter content. The journal's standard [Terms & Conditions](#) and the [Ethical guidelines](#) still apply. In no event shall the Royal Society of Chemistry be held responsible for any errors or omissions in this *Accepted Manuscript* or any consequences arising from the use of any information it contains.

**A polyaniline/graphene nanocomposite prepared by *in situ*  
polymerization of polyaniline onto polyanion grafted graphene and  
its electrochemical properties**

Tao Wu   Xiaoyang Xu   Lei Zhang   Huabin Chen   Jianping Gao\*   Yu Liu

(School of Science, Tianjin University, Tianjin, 300072, P. R. China)

**Abstract:**

Poly(sodium 4-styrenesulfonate), a polyanion, was grafted onto reduced graphene oxide (RGO-g-PSSNa) by *in situ* radical polymerization and was then chemically reduced with hydrazine hydrate. The RGO-g-PSSNa was characterized by infrared, ultraviolet-visible, Raman and x-Ray photoelectron spectroscopies as well as thermogravimetric analysis, scanning electron microscopy and transmission electron microscopy. The results prove that the poly(sodium 4-styrenesulfonate) was grafted onto the reduced graphene oxide nanosheets. RGO-g-PSSNa forms a more stable aqueous suspension than a reduced graphene oxide/poly(sodium 4-styrenesulfonate) blend. The degree of grafting in the RGO-g-PSSNa can be adjusted by changing the amount of the initiator. A polyaniline/RGO-g-PSSNa nanocomposite was prepared by *in situ* polymerization of aniline in the presence of RGO-g-PSSNa, and the electrochemical properties of the composite were studied with cyclic voltammetry.

**1. Introduction**

Graphene was first reported in 2004 [1] and since then it has attracted a great deal of attention because of its excellent electronic [2-7], thermodynamic [8] and mechanical properties [9-13]. There are three main methods to prepare graphene: micro-mechanical stripping [14], chemical vapor deposition [15-17] and chemical redox reactions. The reduction of graphene oxide (GO) is a

---

\* Corresponding authors: Fax: +86 22 274 034 75.

E-mail address: jianpinggao2012@126.com (J.P. Gao).

simple and large scale method to prepare graphene [18-27]. GO is produced from graphite through chemical oxidation and it has many hydrophilic groups, such as hydroxyl, carboxyl and epoxy groups [28].

The hydrophilic groups in GO allow it to be suspended in numerous polar solvents which offers ways of reacting GO with other chemicals and allows GO to be easily modified to meet different requirements. Currently, both non-covalent [29-31] and covalent [32-33] methods are used to modify the surfaces of GO. The former uses organic molecules with  $\pi$  bonds (like phenyl or alkynyl) to coordinate with the extensive  $\pi$  systems of GO. Xu et al. prepared a stable dispersion of graphene using  $\pi$ - $\pi$  coordination between GO and pyrene butyric acid and then they prepared flexible graphene films by filtering the modified GO [34].

Surface modification of GO can also be accomplished by chemical reactions. Both small molecules and macromolecules can be used to functionalize GO. Small molecules such as amine-bearing molecules [35] and diazonium compounds [36] have been successfully bonded to the surface of GO. As for macromolecules, there are mainly two methods to covalently bind them to GO. One is to graft a polymer onto the surface of the GO by reacting the functional groups of GO with the active end-group of the polymer. Zhuang et al. grafted triphenylamine polyazomethines onto the surface of GO by amidation [37]. The other way is to bond an initiator onto the surface of the GO using a chemical reaction and then use the initiator to trigger an in situ chain growth of the monomers to form a polymer grafted GO. Shen et al. designed a process for the assembly of graphene based on layer-by-layer films. First they exfoliated the graphite oxide into individual GO sheets and then they used an in situ reduction to produce individual graphene sheets. Finally, poly(acrylic acid) or poly(acryl amide) were covalently grafted onto the graphene

sheets using in situ living free radical polymerization [38]. They also used the same strategy to prepare amphiphilic graphene nanosheets [39].

Modified graphene usually displays special characteristics, for example it has excellent electrochemical properties, which can be applied to Li batteries, dual cells, and supercapacitors. Supercapacitors have both the high specific energy of galvanic cells and the high specific power of capacitors. The capacity of a supercapacitor is 20 to 200 times higher than that of a traditional capacitor and its specific power is far higher than secondary batteries. Supercapacitors can be prepared by integrating conductive polymers or oxides with GO. Wang et al. fabricated self-assembled multilayered films composed of graphene and azo polyelectrolyte through electrostatic layer-by-layer adsorption. In the multilayered films, the graphene nanosheets were densely packed to form random graphene networks, and the azo polyelectrolyte filled the space in-between the nanosheets [40]. Cheng et al. successfully fabricated binderless supercapacitors with a high specific capacitance by using graphene and MnO<sub>2</sub>-nanoflowers coated with graphene [41].

In this paper, a polyanion of poly(sodium 4-styrenesulfonate) (PSSNa) was grafted onto graphene oxide (RGO-g-PSSNa) by in situ polymerization, and then polyaniline (PANI) was deposited to form PANI/RGO-g-PSSNa nanocomposites. A homogeneous suspension was obtained after PANI was deposited on the surface of RGO-g-PSSNa. However, a heterogeneous solution was only obtained when PANI was directly deposited on the surface of RGO. Therefore, the grafted PSSNa plays an important role in stabilizing the PANI/RGO-g-PSSNa nanocomposites in an aqueous suspension. This property is useful for many potential applications. In this paper, the properties of the PANI/RGO-g-PSSNa composites as supercapacitors were studied.

## 2. Experimental

### 2.1. *Materials*

Graphite was obtained from Huadong Graphite Processing Factory and potassium permanganate was obtained from Xian Chemical Reagent Co. Sodium nitrate, concentrated sulfuric acid, azobisisobutyronitrile (AIBN), N, N-dimethylformamide (DMF), hydrazine hydrate, aniline, anhydrous ethanol, ammonium persulfate, 30% hydrogen peroxide and hydrochloric acid were all purchased from Tianjin Chemical Co. Sodium p-styrene sulfonate (NaSS) was purchased from XZL bio-technology Co. All chemicals were analytical grade and used as received.

### 2.2. *Preparation of GO suspension*

A GO suspension was prepared from purified natural graphite by a modified Hummers method [42, 43]. Briefly, concentrated  $\text{H}_2\text{SO}_4$  (23 mL) was added into a 250-mL flask filled with graphite (1 g) at 0 °C (ice bath), followed by the addition of  $\text{NaNO}_3$  (0.5 g). Then solid  $\text{KMnO}_4$  (3 g) was added gradually with stirring while the temperature of the mixture was kept below 20 °C. The mixture was then stirred with a mechanical stir bar for 2 h. After increasing the temperature to 35 °C and maintaining the temperature for half an hour, excess deionized water was added to the mixture and the temperature was then increase to 90 °C, and stirred for 0.5 h. Finally 30%  $\text{H}_2\text{O}_2$  was added until the color of the mixture changed to brilliant yellow and no more gas was being produced. The product was filtered and washed three times with 5% HCl solution to remove the metal ions and then washed with deionized water to remove the acid. The resulting filter cake was dried in air and then re-dispersed into water. A suspension of GO nanosheets was obtained after the product was sonicated for 3 h in deionized water.

### 2.3. *Preparation of RGO-g-PSSNa*

Graphene oxide nanosheets (20 mg) were dispersed in 50 mL of N,N-dimethylformamide (DMF) and placed in a 100-mL flask. Then 20 mg AIBN and 400 mg NaSS were added to the flask. The flask was placed under a  $\text{N}_2$  atmosphere gas and immersed in an oil bath at 75 °C with vigorous stirring to start the polymerization. After reacting for a certain amount of time (normally

48 h), a precipitate formed and settled to the bottom of the flask. The precipitate was collected by filtration and dried under vacuum at 40 °C for 24 h, and then it was dispersed into distilled water and sonicated for about 15 min to form a suspension. The suspension was then filtered through a microporous membrane (0.45 µm in diameter) and rinsed three times with distilled water to remove the PSSNa homopolymer, which was produced in the polymerization. The filter cake was re-dispersed in the water, and then was reduced with hydrazine hydrate (200 µL, 80%) at 85 °C for 24 h to obtain a homogeneous black dispersion. The insoluble substance (reduced GO) was completely removed by filtration. The filtrate was freeze-dried in a freeze-drying vessel (Alpha1-2, Christ, German) to obtain black RGO-g-PSSNa.

#### **2.4. Preparation of PANI/G-g-PSSNa composites**

First 20 mL hydrochloric acid solution (1 mol/L) and 2 mg of RGO-g-PSSNa were added to a 100-mL flask and sonicated until a homogeneous suspension was obtained. Then a given amount of aniline was added to the flask. Under stirring, the flask was immersed in an ice-water bath for 20 min. Then, 20 mL of aqueous ammonium persulfate solution in a 50-mL constant pressure funnel was slowly added dropwise to the aniline/RGO-g-PSSNa suspension. The flask was then kept at 4 °C for 10 h. The mixture was filtered and rinsed three times with distilled water and anhydrous ethanol. After the resultant filter cake was dried under vacuum at 40 °C for 24 h, the product, PANI/RGO-g-PSSNa, was obtained.

#### **2.5. Characterization**

The RGO-g-PSSNa were allowed to dry under ambient conditions and then they were coated with gold using a sputter coater (Desk-II; Denton Vacuum) before the morphology of the samples was observed by scanning electron microscopy (SEM) (JSM-6700F). The samples for transmission electron microscopy (TEM) were prepared by dropping the GO aqueous suspension onto a carbon coated copper grid. They were dried under ambient conditions prior to being

introduced into the TEM (Tecnaï G2 F20) chamber. The Infrared spectra (IR) of the GO and RGO-g-PSSNa were measured with a Perkin-Elmer Paragon-1000 FT-IR spectrometer in the range of 500-4000  $\text{cm}^{-1}$ . Each FT-IR spectra was the average of 20 scans.

Ultraviolet-visible (UV-Vis) absorption spectra of the aqueous GO and RGO-g-PSSNa solutions were recorded with a TU-1901 UV-Vis spectrophotometer. X-ray diffraction (XRD) spectra of the graphite, GO and RGO-g-PSSNa were measured using an x-ray diffractometer (X'pert, PANalytical) with a reference target: Co K $\alpha$  radiation ( $\lambda=1.73\text{\AA}$ ), voltage: 40 kV, and current: 300 mA. The films were measured from 3 to 80° (2 $\theta$ ) with scan speed 0.02 °/s. Elemental analysis, including the content of carbon, sulfur and oxygen in graphene, GO and RGO-g-PSSNa, was conducted with an x-ray photoelectron spectrometer (XPS, PHI1600 ESCA System, PERKIN ELMER, USA). Raman measurements were performed with a Raman microscope (DXR Raman Microscope, Thermo Scientific) equipped with EZ OMNIC software, in a backscattering configuration. Raman spectra were obtained with a power output of 0.5 mW at the sample. All spectra were baseline corrected, averaged, and smoothed. RGO-g-PSSNa was first dried to a constant weight in a vacuum at 60 °C, and then the thermogravimetric diagram of the RGO-g-PSSNa material was measured with a Rigaku-TD-TDA analyzer using a heating rate of 6 °C /min.

A working electrode containing PANI/RGO-g-PSSNa was prepared by using carbon black as the conductive agent and polytetrafluoroethene as the binder. The mass ratio of carbon black, polytetrafluoroethene and PANI/RGO-g-PSSNa was 20:5:75. They were put into a mortar, along with an adequate amount of anhydrous ethanol, and ground to form a paste. Foam nickel pieces (1 cm $\times$ 1 cm) were coated with the paste so that each piece contained 5 to 8 mg of active substance (PANI/RGO-g-PSSNa), and then they were dried in the air and pressed into the working electrode

with a pressure of 10 MPa.

The electrochemical properties and capacitance of the PANI/G-g-PSSNa electrodes were studied using a three-electrode system in a 7 M KOH aqueous electrolyte solution by cyclic voltammetry (CV) [41, 44]. The CV response of the electrodes was measured at different scan rates varying from 5 to 100  $\text{mV}\cdot\text{s}^{-1}$ . The experiments were performed using an EG&G Princeton Applied Research VMP3 work station controlled by a computer.

### 3. Results and Discussion

#### 3.1. Preparation and analysis of RGO-g-PSSNa

The GO nanosheets used for preparing RGO-g-PSSNa were prepared in our laboratory. Their aqueous suspensions are stable for several months with no precipitation occurring. The nanosheets can also be suspended in DMF and dimethyl sulfoxide, implying that the GO nanosheets are hydrophilic and small enough to be suspended in numerous polar solvents, which has been further confirmed by TEM, XRD, and XPS [43]. Stable GO aqueous suspensions offers mediums for chemical reactions and the functional groups on the GO nanosheets provide places for grafting polymerization.

#### 3.2. IR spectra (FTIR) of RGO-g-PSSNa

RGO-g-PSSNa was prepared by in situ polymerization. In order to determine if the PSSNa has been grafted onto the RGO, infrared spectra of RGO, PSSNa and RGO-g-PSSNa were taken and are shown in Fig. 1. For the IR spectrum of PSSNa, the peak near  $3400\text{ cm}^{-1}$  is an O-H stretching vibration which results from the hydrolysis of sodium sulfonate; the peak near  $1700\text{ cm}^{-1}$  is an S=O stretching vibration; the peaks near  $1500\text{ cm}^{-1}$  are characteristic absorption peaks for benzene and the two peaks in the fingerprint region indicate a para-substitution of sodium sulfonate; the peaks between  $1000$  and  $1250\text{ cm}^{-1}$  are characteristic C-C absorption peaks for a carbon skeleton in a macromolecular chain. In the RGD spectrum, the absorption peaks at about

3400, 2900, 1700 and 1500  $\text{cm}^{-1}$  all overlap with those of PSSNa. The IR spectrum of the black RGO-g-PSSNa has the same characteristic absorption peaks as PSSNa. These results indicate that PSSNa has grafted onto the surface of graphene, because the PSSNa homo-polymer has been removed.

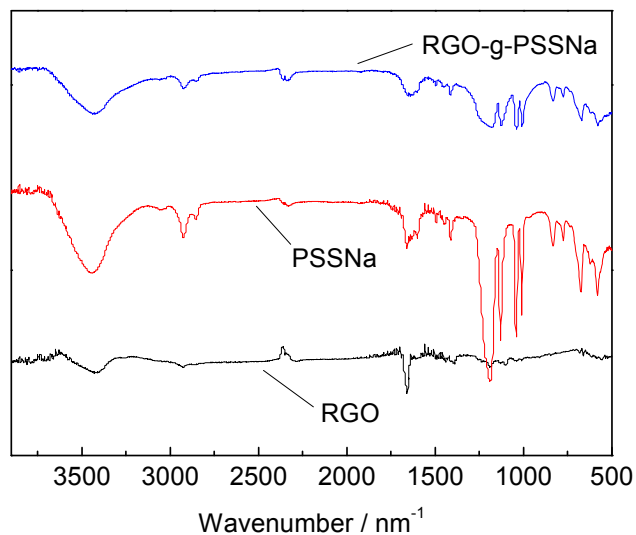


Fig. 1 - IR spectra (FTIR) of RGO, PSSNa and RGO-g-PSSNa.

### 3.3. UV-Vis spectra of RGO-g-PSSNa aqueous solutions

UV-Vis spectra of RGO-g-PSSNa aqueous suspensions with different concentrations were measured in the wavelength range of 200 to 400 nm (Fig. 2a). The characteristic absorption peaks located at 180, 225, and 270 nm indicate the existence of benzene rings that come from PAANA. The linear relationship between the absorbance at 225 nm and the RGO-g-PSSNa concentration (Fig. 2b) is in accordance with Beer's law (the absorptivity is  $35.9 \text{ L}\cdot\text{g}^{-1}\cdot\text{cm}^{-1}$ ), so the RGO-g-PSSNa suspension is a stable suspension. The UV-Vis data further indicates that PSSNa has grafted onto the surface of the graphene.

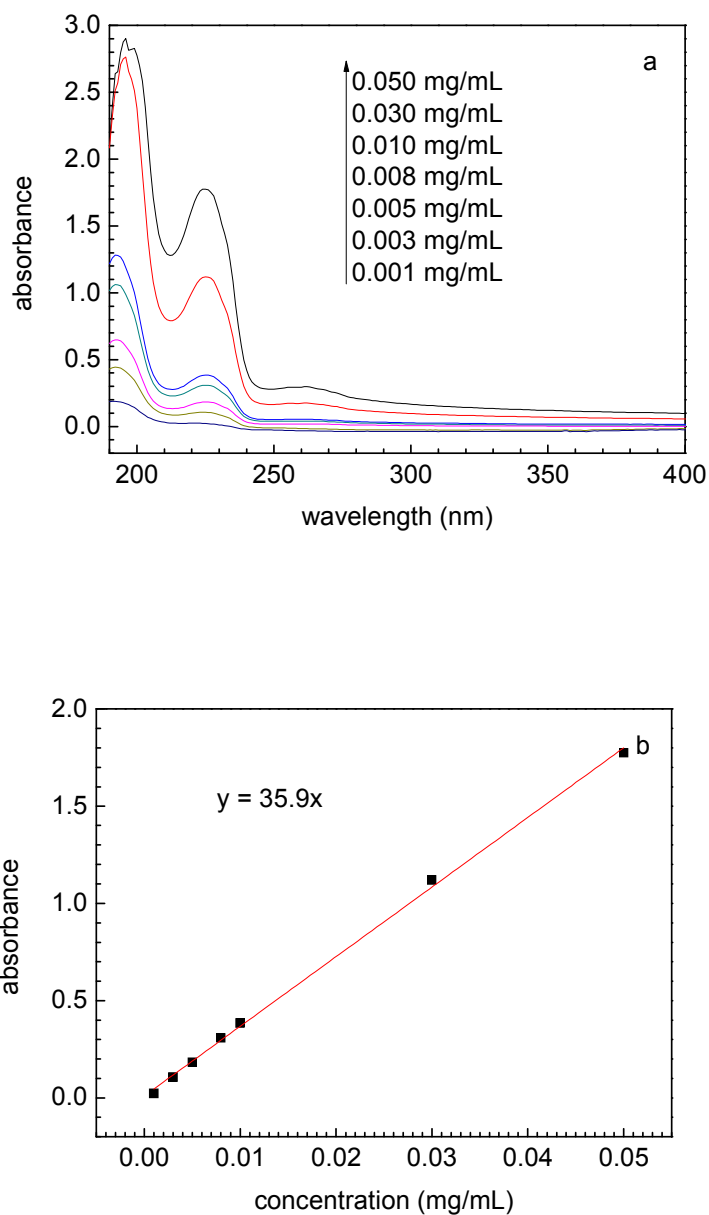


Fig. 2 - UV-Vis spectra of RGO-g-PSSNa concentrations (a) and calibration curve of

RGO-g-PSSNa (b).

### 3.4. Raman analysis of RGO-g-PSSNa

Fig. 3 shows the Raman spectra of graphite, GO and RGO-g-PSSNa. The Raman spectra of GO has wide peaks around 1600 (G) and 1350  $\text{cm}^{-1}$  (D). RGO-g-PSSNa also has these D and G

peaks but the D/G intensity ratio (0.93) is bigger than that (0.85) in the GO spectrum. This indicates that the GO in the RGO-g-PSSNa has been reduced, which is further proved by the XRD analysis.

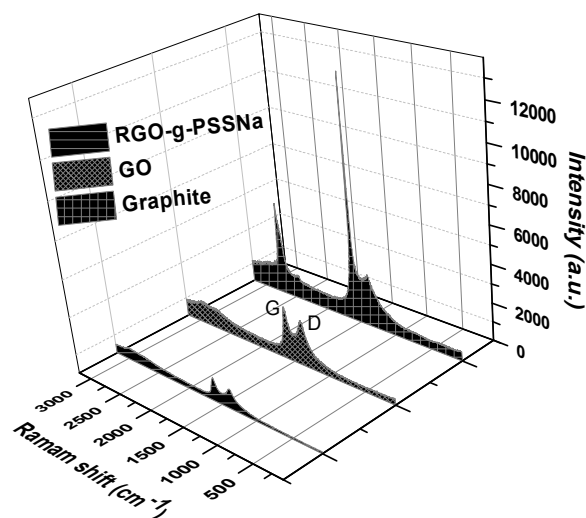


Fig. 3 - Raman spectra of graphite, GO, and RGO-g-PSSNa.

### 3.5. XRD analysis of RGO-g-PSSNa

The XRD spectra for graphite, GO and RGO-g-PSSNa are shown in Fig. 4. For the graphite sample, there is one very strong, sharp 002 diffraction peak near  $27^\circ$ . In the GO spectrum, this peak is greatly reduced and a new strong peak at about  $10^\circ$  appears in the XRD spectrum. This is because the graphite structure is destroyed upon oxidation. However, this new peak is not present in the spectrum of RGO-g-PSSNa which indicates that GO was reduced by the hydrazine hydrate reaction. This confirms the existence of RGO in the RGO-g-PSSNa product. The IR, UV-Vis and Raman results, all confirm the structure and composition of RGO-g-PSSNa. It contains both RGO and PSSNa and they are linked by chemical bonds, so PSSNa has been grafted onto the GO nanosheets.

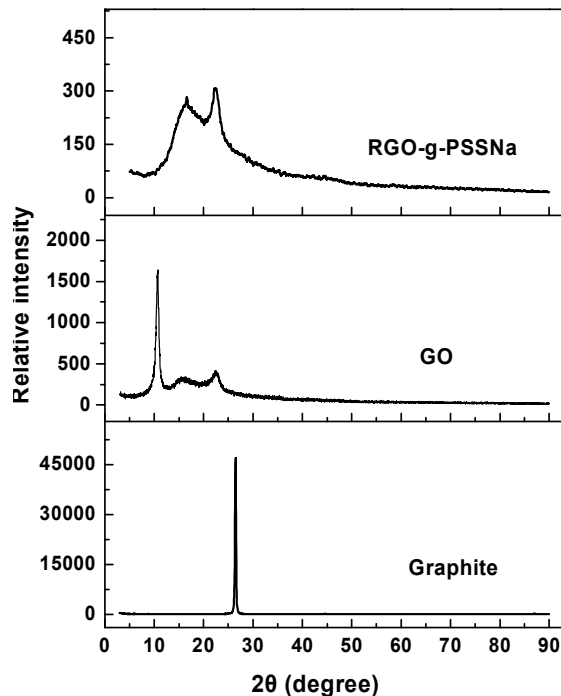


Fig. 4 - XRD patterns of RGO-g-PSSNa, GO, and natural graphite.

### 3.6. XPS analysis of RGO-g-PSSNa

XPS is an effective way to analyze carbon materials. Several RGO-g-PSSNa samples were prepared using different amounts of initiator during the *in situ* polymerization and the XPS spectra for the 20- and 100-mg samples are shown in Fig 5. Their respective sulfur contents are 2.9% and 2.4%. The calculated grafting degrees ( $m(\text{PSSNa})/m(\text{RGO-g-PSSNa})$ ) are 18.6% and 15.4%, respectively. The number of active sites on the surface of GO that are available for grafting is fixed, so the degree of grafting is determined by the length of the graft chain when there is excess monomer present. More initiator produces shorter PSSNa chains which causes a lower degree of grafting. So the grafting degree of RGO-g-PSSNa can to a certain extent be adjusted by changing the amount of initiator. At the same time, the C/O ratios (carbon to oxygen atoms) of GO in the two RGO-g-PSSNa samples are 4.34 and 4.94 respectively after subtracting the amount from PSS. The ratios of carbon-carbon bonds to carbon-oxygen bonds (C-C/C-O) are 6.4 and 4.2 respectively.

Since the C/O and C-C/C-O ratios of GO in the two RGO-g-PSSNa samples are both higher than those in the original GO (C/O: 2.72; C-C/C-O: 1.6), the GO is highly reduced.

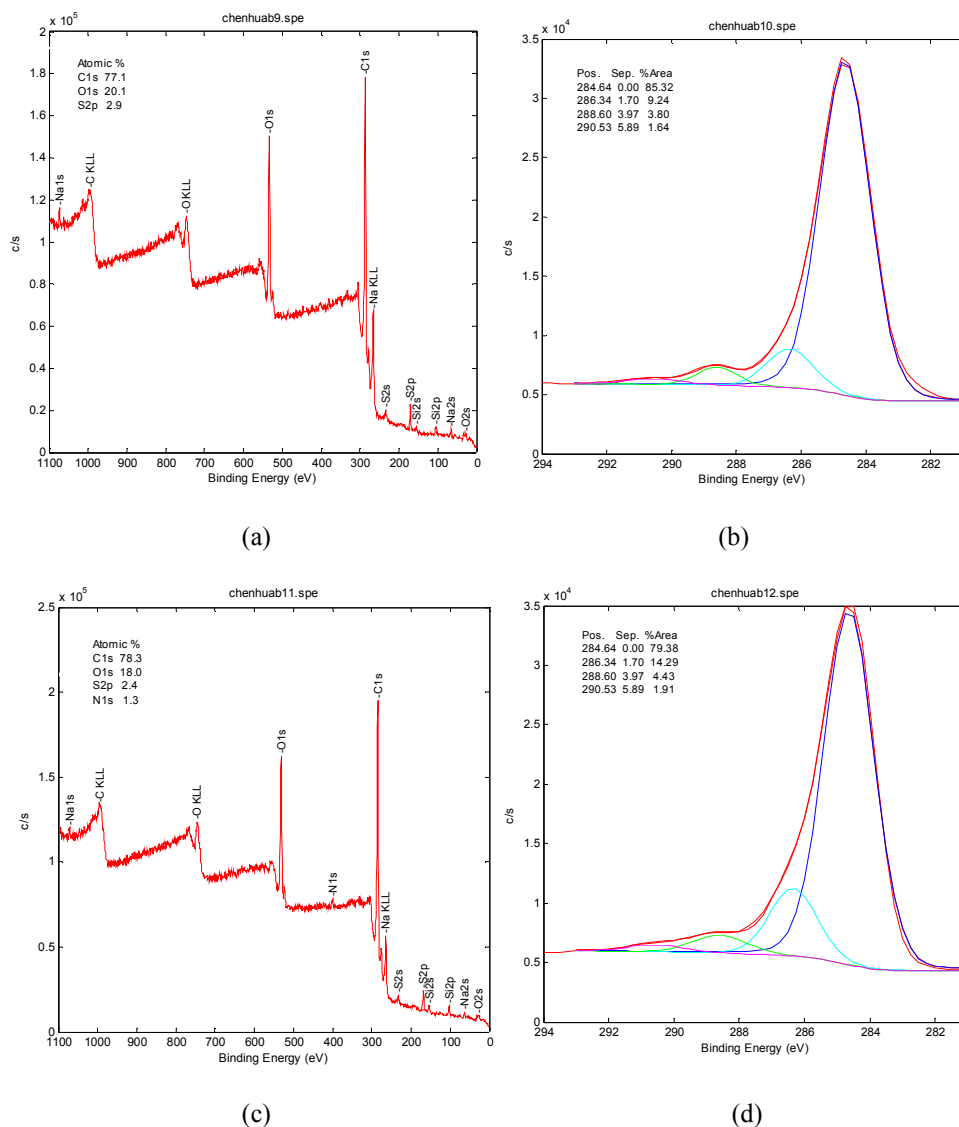


Fig. 5 - XPS spectra of RGO-g-PSSNa which prepared with 20 mg of initiator (a); deconvolution of C1s spectra of (a) (b); XPS spectra of RGO-g-PSSNa which prepared with 100 mg or initiator (c); deconvolution of C1s spectra of (c) (d).

### 3.7. TGA analysis of RGO-g-PSSNa

Fig. 6 shows the TGA curves of RGO and RGO-g-PSSNas prepared by adding different amounts of initiator, 20, 40 or 100 mg. This measurement was conducted under a flow of nitrogen.

For RGO, there is an 8% mass loss before 200 °C, and the total mass loss is about 20%, indicating that RGO is well reduced. When PSSNa is grafted onto RGO, there is an obvious mass loss starting at 430 °C and it lasts until 1000 °C. This huge mass loss is caused by decomposition of the grafted chains, PSSNa. The 20-mg initiator RGO-g-PSSNas sample has a higher total mass loss than the 40- and 100-mg samples. This indicates that less initiator produces longer PSSNa chains which causes a higher degree of grafting.

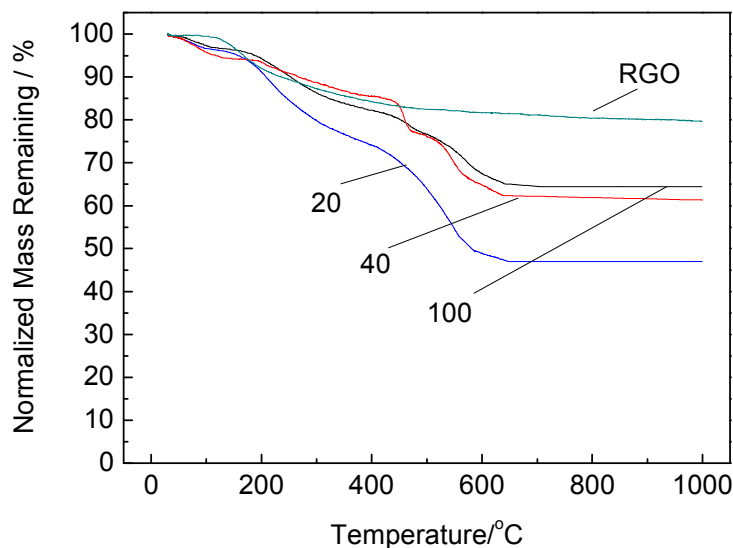


Fig. 6 - TGA curves of RGO and RGO-g-PSSNa made with different amounts of initiator.

### 3.8. Structure characterization of RGO-g-PSSNa

Fig. 7 shows a TEM photo of RGO-g-PSSNa which has both crystalline and amorphous regions. The lattice width in the crystalline region is 0.34 nm, which is characteristic of graphene. The amorphous region contains the PSSNa. Since PSSNa is on the top surface of the RGO nanosheets, the RGO crystalline lattice is partly covered.

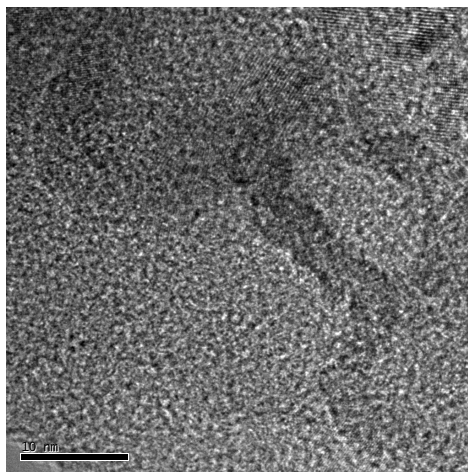


Fig. 7 - TEM image of RGO-g-PSSNa.

Fig. 8 - shows the SEM photo of dried RGO-g-PSSNa particles. They are bigger than the original GO nanosheets, and their surface is not smooth. Their thickness is about 5-10 nm which is thicker than GO nanosheets. This suggests that each RGO-g-PSSNa particle contains many RGO nanosheets which are stuck together by PSSNa, which has been grafted onto the RGO nanosheets. So RGO-g-PSSNa can form a film when a RGO-g-PSSNa suspension is coated on a glass slide.

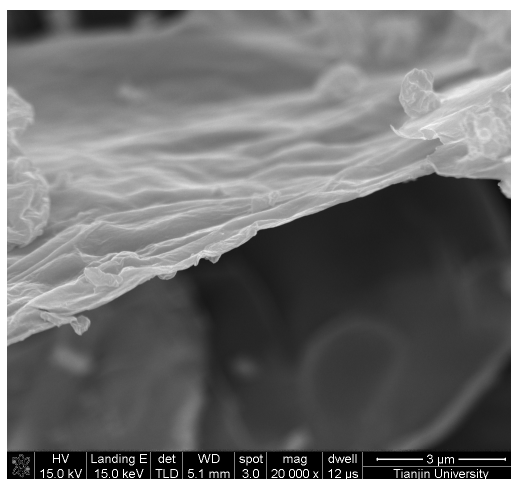


Fig. 8 - SEM images of RGO-g-PSSNa.

Fig. 9 shows the optical photos of aqueous suspensions of RGO, a blend of RGO and PSSNa (RGO-b-PSSNa, GO reduced in the presence of PSSNa) and RGO-g-PSSNa. RGO-b-PSSNa and RGO-g-PSSNa are well dispersed in water, whereas RGO does not disperse at all. After three days,

the RGO-b-PSSNa suspension coagulates, whereas no coagulation occurs in the RGO-g-PSSNa suspension. So the RGO-g-PSSNa suspension is more stable than the RGO-b-PSSNa suspension. Moreover, the RGO-g-PSSNa suspension is stable for at least five months without any precipitation occurring. This indicates that the grafted PSSNa chains stabilize the RGO-b-PSSNa suspension.

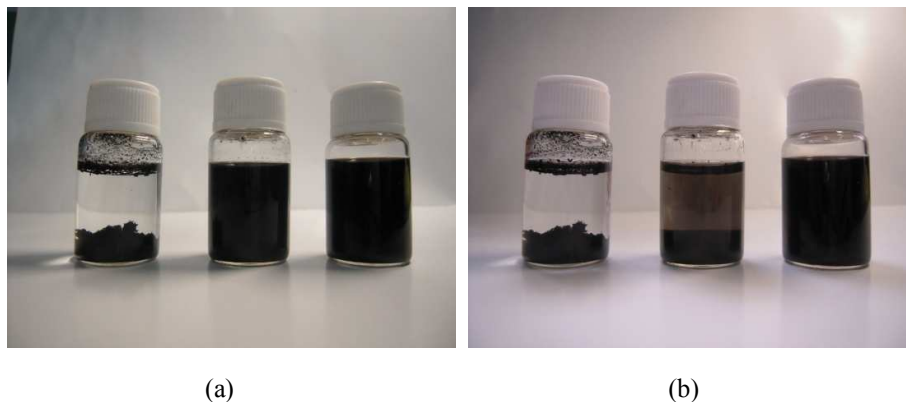
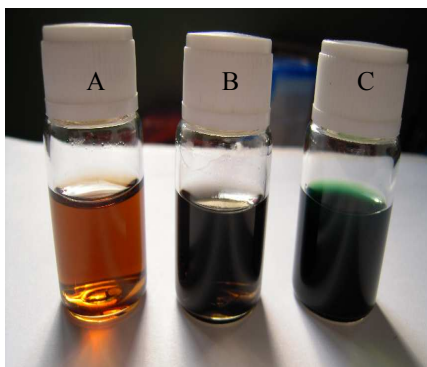


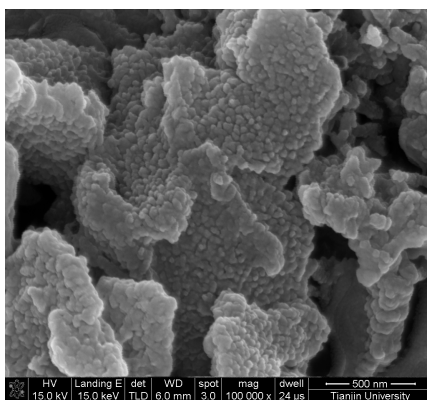
Fig. 9 - Optical photos of reduced GO (RGO), RGO-b-PSSNa and RGO-g-PSSNa in water over time. initial(a); 3 days later (b).

### 3.9. Structure characterization of PANI/RGO-g-PSSNa

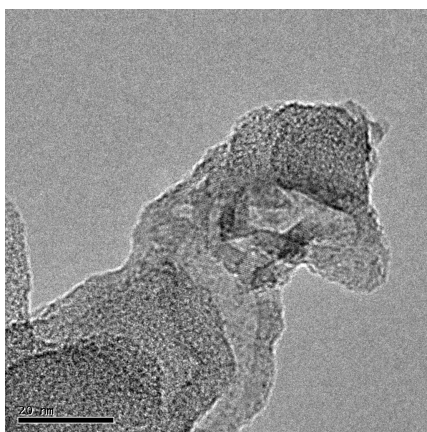
Fig. 10 shows the optical photo of the PANI/RGO-g-PSSNa nanocomposites suspension, the SEM and TEM photos of the PANI/RGO-g-PSSNa nanocomposites. A homogeneous suspension has been obtained after PANI was deposited on the surface of RGO-g-PSSNa. However, we can only get a heterogeneous suspension when PANI was deposited on the surface of RGO. Therefore, the PSSNa that has been grafted on the surface of RGO plays an important role in stabilizing the PANI/RGO-g-PSSNa nanocomposites in aqueous suspension, as illustrated in Fig.11.



(a)



(b)



(c)

Fig. 10 - The optical photos of GO (A), RGO-g-PSSNa (B) and PANI/RGO-g-PSSNa (C) (a);

the SEM (b) and TEM (c) images of PANI/RGO-g-PSSNa.

They have similar sizes with GO, but are much thicker, because many mono-dispersed small particles are deposited on the RGO surface. The particles are PANI and they are about 40 nm. The

PANI particles are amorphous whereas the RGO is crystalline with a lattice width of 0.34 nm as shown in the TEM photo.

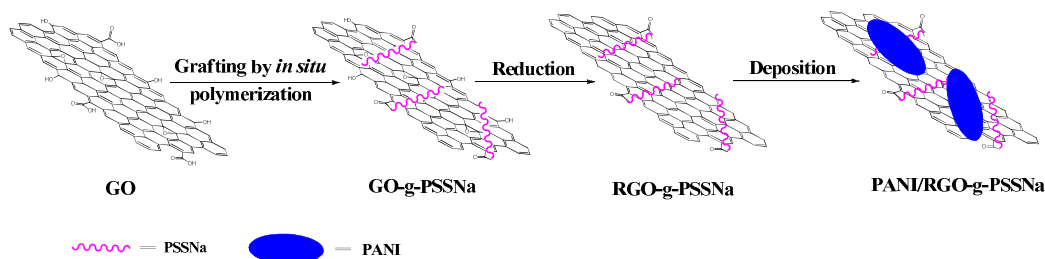


Fig. 11. Illustration of the formation process of PANI/RGO-g-PSSNa.

### 3.10. Raman analysis of PANI/RGO-g-PSSNa

Fig. 12 shows the Raman spectra of PANI/RGO-g-PSSNa and RGO-g-PSSNa. They both have two wide peaks at 1355(D) and 1595  $\text{cm}^{-1}$  (G). The fact that the intensity of the D peak is similar to that of the G peak indicates that defects or partly amorphous random structures exist in the RGO-g-PSSNa. Since PANI has peaks at 1300 and 1600  $\text{cm}^{-1}$  and the intensity of the latter is stronger than the former, the Raman spectrum of PANI/RGO-g-PSSNa is a superposition of the RGO-g-PSSNa and PANI spectra. The D/G intensity ratio of PANI/RGO-g-PSSNa was decreased to 0.87 compared to that of RGO-g-PSSNa due to the enhancement of the peak intensity at 1600  $\text{cm}^{-1}$  by PANI, which has many  $\pi$  bonds [45, 46].

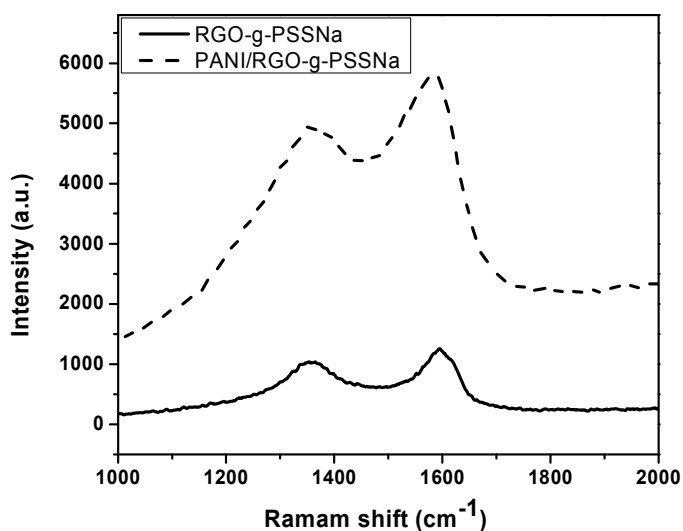


Fig. 12 - Raman spectra of PANI/RGO-g-PSSNa, RGO-g-PSSNa.

### 3.11. *The electrochemical properties of the PANI/RGO-g-PSSNa*

Since the PANI/RGO-g-PSSNa nanocomposites are well dispersed in water, it offer a feasibility to process them into films or electrodes. Here, we take a supercapacitor as an example to investigate the electrochemical properties of the PANI/RGO-g-PSSNa. The CVs for a PANI/RGO-g-PSSNa electrode at different scan rates, 5, 10, 20, 50 and 100  $\text{mV}\cdot\text{s}^{-1}$  is showed in Fig. 13. The scans were conducted in a 7 M KOH solution. There are two redox peaks in each curves which can be attributed to the redox transitions of PANI between a semiconducting state and a conducting state.<sup>42</sup> The redox peaks in each curve are symmetric which indicates that the sample electrode has good reversibility in a potassium hydroxide solution. The specific capacitance of the sample was  $768 \text{ F}\cdot\text{g}^{-1}$  (for a scan rate of 5  $\text{mV}/\text{s}$ ) according to the principle of CV [47], which is higher than that for pure PANI ( $46 \text{ F}\cdot\text{g}^{-1}$ ) [48]. This result demonstrates that the dispersion of nanoscale PANI particles on RGO reduces the diffusion and migration length of the electrolyte ions during the fast charge/discharge process. Besides, RGO in the composite can provide an electron transfer path owing to its good conductivity. The CV curves of PANI/RGO-g-PSSNa electrode at different scan rates shows the cathodic peaks shift and the anodic peaks shift negatively with the increment of potential sweep rates from 5 to 100  $\text{mV}\cdot\text{s}^{-1}$ , which is due to the resistance of the electrode [47]. In addition, the increase of current with scan rates shows a good rate capability for PANI/RGO-g-PSSNa nanocomposite electrode.

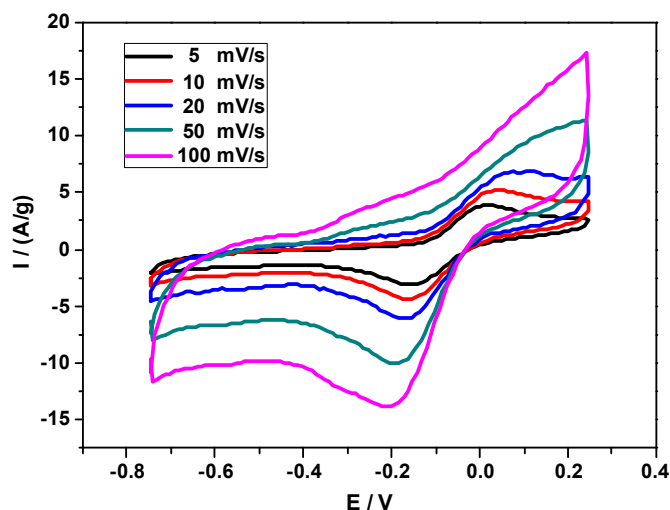


Fig. 13 - CV curves of PANI/RGO-g-PSSNa electrode at different scan rates.

#### 4. Conclusions

RGO-g-PSSNa was prepared through *in situ* radical polymerization and then chemical reduction with hydrazine hydrate was performed. RGO-g-PSSNa shows a more stable aqueous suspension than a RGO/PSSNa blends. The degree of grafting of RGO-g-PSSNa can be adjusted by changing the amount of initiator, that is, more initiator produces shorter PSSNa chains which cause a lower grafting degree. A stable PANI/RGO-g-PSSNa nanocomposite suspension was prepared by *in situ* polymerization of PANI in the presence of RGO-g-PSSNa and it shows extraordinary electrochemical properties. This stable suspension can be also easily used to prepare film materials for electrode that can apply in Li batteries, solar batteries and so on.

#### Acknowledgments

This work was supported by the National Science Foundation of China (21074089, 50603017) and Tianjin Municipal Science and Technology Commission, P. R. China (09JCZDJC23300).

#### References

- 1 K. S. Novoselov, A. K. Geim, S. V. Morozov, D. Jiang, M. I. Katsnelson, I. V. Grigorieva, S.

- V. Dubonos, A. A. Firsov, *Nature*, 2005, **438**, 197.
- 2 Y. Zhang, J. W. Tan, H. L. Stormer, P. Kim, *Nature*, 2005, **438**, 201.
- 3 J. C. Meyer, A. K. Geim, M. I. Katsnelson, K. S. Novoselov, T. J. Booth, S. Roth, *Nature*, 2007, **446**, 60.
- 4 H. B. Heersche, P. Jarillo-Herrero, J. B. Oostinga, L. M. K. Vandersypen, A. F. Morpurgo, *Nature*, 2007, **446**, 56.
- 5 T. Ohta, A. Bostwick, T. Seyller, K. Horn, E. Rotenberg, *Science*, 2006, **313**, 951.
- 6 R. M. Westervelt, *Science*, 2008, **320**, 324.
- 7 K. S. Novoselov, Z. Jiang, Y. Zhang, S. V. Morozov, H. L. Stormer, U. Zeitler, J. C. Maan, G. S. Boebinger, P. Kim, A. K. Geim, *Science*, 2007, **315**, 1379.
- 8 A. A. Balandin, S. Ghosh, W. Bao, I. Calizo, D. Teweldebrhan, F. Miao, C. N. Lau, *Nano Lett.*, 2008, **8**, 902.
- 9 S. Stankovich, D. A. Dikin, G. H. B. Dommett, K. M. Kohlhaas, E. J. Zimney, E. A. Stach, R. D. Piner, S. T. Nguyen, R. S. Ruoff, *Nature*, 2006, **442**, 282.
- 10 D. A. Dikin, S. Stankovich, E. J. Zimney, R. D. Piner, G. H. B. Dommett, G. Evmenenko, S. T. Nguyen, R. S. Ruoff, *Nature*, 2007, **448**, 457.
- 11 D. Li, R. B. Kaner, *Science*, 2008, **320**, 1170.
- 12 C. Lee, X. Wei, J. W. Kysar, J. Hone, *Science*, 2008, **321**, 385.
- 13 J. S. Bunch, A. M. van der Zande, S. S. Verbridge, I. W. Frank, D. M. Tanenbaum, J. M. Parpia, H. G. Craighead, P. L. McEuen, *Science*, 2007, **315**, 490.
- 14 K. S. Novoselov, A. K. Geim, S. V. Morozov, D. Jiang, Y. Zhang, S. V. Dubonos, I. V. Grigorieva, A. A. Firsov, *Science*, 2004, **306**, 666.

- 15 M. Eizenberg, J. M. Blakely, *Surf. Sci.*, 1970, **82**, 228.
- 16 T. Aizawa, R. Souda, S. Otani, Y. Ishizawa, C. Oshima, *Phys. Rev. Lett.*, 1990, **64**, 768.
- 17 K. S. Kim, Y. Zhao, H. Jang, S. Y. Lee, J.M. Kim, K. S. Kim, J. H. Ahn, P. Kim, J. Y. Choi, B. H. Hong, *Nature*, 2009, **457**, 706.
- 18 H. C. Schniepp, J. L. Li, M. J. McAllister, H. M. Sai, Herrera-Alonso, D. H. Adamson, R. K. Prud'homme, R. Car, D. A. Saville, I. A. Aksay, *J. Phys. Chem. B.*, 2006, **110**, 8535.
- 19 M. J. McAllister, J. L. Li, D. H. Adamson, H. C. Schniepp, A. A. Abdala, J. Liu, M. Herrera-Alonso, D. L. Milius, R. Car, R. K. Prud'homme, I. A. Aksay, *Chem. Mater.*, 2007, **19**, 4396.
- 20 S. Stankovich, D. A. Dikin, R. D. Piner, K. A. Kohlhaas, A. Kleinhammes, Y. Jia, Y. Wu, S. T. Nguyen, R. S. Ruoff, *Carbon*, 2007, **45**, 1558.
- 21 S. Stankovich, R. D. Piner, X. Chen, N. Wu, S. T. Nguyen, R. S. Ruoff, *J. Mater. Chem.*, 2006, **16**, 155.
- 22 C. Gomez-Navarro, R. Thomas Weitz, A. M. Bittner, M. Scolari, A. Mews, M. Burghard, K. Kern, *Nano Lett.*, 2007, **7**, 3499.
- 23 X. Wang, L. Zhi, K. Mullen, *Nano Lett.*, 2008, **8**, 323.
- 24 S. Gilje, S. Han, M. Wang, K. L. Wang, R. B. Kaner, *Nano Lett.*, 2007, **7**, 3394.
- 25 X. Fan, W. Peng, Y. Li, X. Li, S. Wang, G. Zhang, F. Zhang, *Adv. Mater.*, 2008, **20**, 4490.
- 26 H. A. Becerril, J. Mao, Z. Liu, R. M. Stoltenberg, Z. Bao, Y. Chen, *ACS Nano.*, 2008, **2**, 463.
- 27 G. Eda, G. Fanchini, M. Chhowalla, *Nat. Nanotechnol.*, 2008, **3**, 270.
- 28 H.Y. He, J. Klinowski, M. Forster, *Chem. Phys. Lett.*, 1998, **287**, 53.
- 29 W. S. Ma, L. Wu, F. Yang, S. F. Wang, *J. Mater. Sci.*, 2014, **49**, 562.

- 30 F. M. Koehler, A. Jacobsen, K. Ensslin, C. Stampfer, W. J. Stark, *Small*, 2010, **6**, 1125.
- 31 P. K. Chow, O. Eksik, N. Koratkar, *Part. Part. Syst. Charact.*, 2013, DOI: 10.1002/ppsc.201300206
- 32 M. M. Stylianakisa, G. D. Spyropoulosa, E. Stratakisa, E. Kymakis, *Carbon*, 2012, **50**, 5554.
- 33 M. M. Stylianakis, E. Stratakis, E. Koudoumas, E. Kymakis, S. H. Anastasiadis, *ACS Applied Mater. Interfaces*, 2012, **4**, 4864.
- 34 29 Y. X. Xu, H. Bai, G. W. Lu, *J. Am. Chem. Soc.*, 2008, **130**, 5856.
- 35 30 A. Sinitskii, A. Dimiev, D. A. Corley, A. A. Fursina, D. V. Kosynkin, J. M. Tour, *ACS Nano*, 2010, **4**, 1949.
- 36 31 M. C. Hsiao, S. H. Liao, M. Y. Yen, P. I. Liu, N. W. Pu, C. A. Wang, C. C. Ma, *ACS Appl. Mater. Interfaces*, 2010, **2**, 3092.
- 37 32 X. D. Zhuang, Y. Chen, G. Liu, *Adv. Mater.*, 2010, **22**, 1731.
- 38 33 J. F. Shen, Y. Z. Hu, C. Li, *Langmuir*, 2009, **25**, 6122.
- 39 34 J. F. Shen, Y. H. Hu, C. Li, *Small*, 2009, **5**, 82.
- 40 35 D.R. Wang, X.G. Wang, *Langmuir*, 2011, **27**,2007.
- 41 36 Q. Cheng, J. Tang, J. Ma , H. Zhang , N. Shinya , L.C. Qin , *Carbon* ,2011,49,2917.
- 42 37 W. Hummers, R. Offeman, *J. Am. Chem. Soc.*, 1958, **80**, 1339.
- 43 38 N.N. Zhang, H.X. Qiu, Y.M. Si, W.Wang , J.P. Gao., *Carbon*, 2011,**49**, 827.
- 44 39 J. Insoo, C. Jinsub, T. Yongsug ,*J. Mater. Chem.*, 2010, **20**, 6164.
- 45 40 D.H. Deng, X.L. Pan, L. Yu, Y. Cui, Y.P. Jiang, J. Qi, W.X. Li, Q. Fu, X.C. Ma, Q.K. Xue, G.G. Sun, X.H. Bao., *Chem. Mater.*, 2011, **23**, 1188.
- 46 41 T. Suai, A. Kaskela, Z. Zhu, P. Ayala, R. Arenal, Y. Tian, P. Laiho, J. Mali, A. G. Nasibulin,

H. Jiang, G. Lanzani, O. Stephan, K. Laasonen, T. Pichler, A. Loiseau, E. I. Kauppinen.,

*Chem. Mater.*, 2011, **23**, 2201.

47 42 Y. G. Wang, H.Q. Li, and Y.Y. Xia , *Adv. Mater.*, 2006, **18**, 2619.

48 43 J. Yan, T. Wei, B. Shao, Z.J. Fan, W.Z. Oian, M.L. Zhang and F. Wei., *Carbon*, 2010, **48**,

487.